A broadly applicable function for describing luminescence dose response

C. I. Burbidge

A broadly applicable function for describing luminescence dose response

C. I. Burbidge[1,2,a)]
[1]*C²TN, Instituto Superior Técnico, Universidade de Lisboa, 2695-066 Bobadela-LRS, Portugal*
[2]*GeoBioTec, Universidade de Aveiro, Campus Universitário de Santiago, 3810-193 Aveiro, Portugal*

The basic form of luminescence dose response is investigated, with the aim of developing a single function to account for the appearance of linear, superlinear, sublinear, and supralinear behaviors and variations in saturation signal level and rate. A function is assembled based on the assumption of first order behavior in different major factors contributing to measured luminescence-dosimetric signals. Different versions of the function are developed for standardized and non-dose-normalized responses. Data generated using a two trap two recombination center model and experimental data for natural quartz are analyzed to compare results obtained using different signals, measurement protocols, pretreatment conditions, and radiation qualities. The function well describes a range of dose dependent behavior, including sublinear, superlinear, supralinear, and non-monotonic responses and relative response to α and β radiation, based on change in relative recombination and trapping probability affecting signals sourced from a single electron trap. © 2015 AIP Publishing LLC.
[http://dx.doi.org/10.1063/1.4927214]

I. INTRODUCTION AND AIMS

Luminescence dosimetry measures delayed phosphorescence, based on the metastable accumulation of electrons and holes in defects of crystalline insulators following primary ionizing irradiation and the recombination of a proportion of these following their liberation by secondary "irradiation"[1] by photons (optically stimulated luminescence, OSL) or phonons (thermally stimulated luminescence, TSL). Variation of signal as a function of absorbed dose for a given set of conditions (material, radiation quality, etc.) may be termed its dose response characteristic (DRC). A variety of forms of DRC have been categorized as linear, superlinear, sublinear, and supralinear.[2,3] To describe these, quadratic, power, or linear approximations have been made at low doses and saturating exponential fits at moderate doses.[4–9] At higher doses, linear and saturating exponential components are often summed or localized fits of simpler form are used.[10–13] Experimental observations and modelling of superlinear behavior[2–6,14–18] and non-monotonic DRCs[10,19–21] show that changes in trapping and/or recombination probability produce significant effects not described by sums of signal components.

TSL and OSL DRCs are experimentally evaluated either by measuring different subsamples following irradiation with a range of doses (multiple aliquot protocol) or by repeated irradiation and measurement of the same subsample (single aliquot protocol).[1,22] The precision of multiple aliquot DRCs and the reproducibility of the repeat single aliquot measurements are enhanced by normalization of the signal response (I) of each subsample to dose (D) relative to their response (I_T) to a fixed "normalization dose" or "test dose" (D_T), which may be delivered prior to or following each dose.[3,8,23–26] Following irradiation and prior to each measurement, samples are commonly "preheated" to redistribute electrons and holes, from traps with low average thermal lifetimes of charge retention.[1,22] Irradiation, pretreatment, relaxation, and measurement alter the distribution of centers and charge populations available for further trapping and recombination;[4,28–32] so, DRCs vary as a function of dose, predose, and non-dose dependent factors, and so does the relationship between I and I_T. Synthetic luminescence dosemeter crystals and natural mineral crystals vary strongly in the types, concentrations, proximities/interrelationships, and thermal stabilities of centers available for charge trapping.[1–3,15,18,29–36]

An accurate broadly applicable function for describing luminescence dose response should reflect common basic behavioral patterns in the signals and materials under analysis, i.e., minimal basic elements of models used to simulate these behaviors. Fits made with such a function could approximate the general form of the luminescence DRC, aid quantification, and interpretation of luminescence-dosimetric processes and improve estimates of absorbed dose. The present study has the aim of developing a single function to account for linear, superlinear, sublinear, and supralinear behaviors and variations in saturation signal level and rate of increase in signal with dose. Its objectives are (i) to describe and test the behavior of the function and its components with reference to a two trap two center numerical model, (ii) to evaluate its application to experimentally observed non-monotonic dose response characteristics, and (iii) to account for changes during D_T and I_T that do not depend on D, for differences in redistribution of charges by preheating and differences in linear energy transfer (LET) between irradiations.

II. CALCULATIONS AND RESULTS

A. Saturating exponential DRC

For phosphorescence signals of first order kinetics, with temperature dependence well described by the Arrhenius

a)E-mail: christoph@ctn.ist.utl.pt

equation, signal decay with time and signal increase with dose follow exponential forms.[2,37] The DRC for a TSL (or OSL) signal based on a one trap one center model (OTOR) including a relaxation period follows a single saturating exponential (McKeever Ch 3.4[2]) with the variables: signal intensity (I) and dose (D), and the parameters: signal intensity at $D = \infty$, i.e., at saturation (I_∞) and $\bar{D}$.[27] By analogy with mean lifetime in radioactive decay and the time constant of a series RC circuit or other damped oscillator (τ), $\bar{D}$ may be viewed as the average dose for which a type of center that will subsequently contribute to signal I is available before being occupied by charge ("average dose of signal saturation"). A non-dose dependent signal component I_0 is also often present

$$I = I_0 + I_\infty(1 - e^{-D/\bar{D}}), \tag{1}$$

$$\frac{dI}{dD} = \frac{I}{D} e^{-D/\bar{D}}. \tag{2}$$

Here, I_∞ acts as a simple multiplier of I (1) and is subsumed in its gradient dI/dD (2), whereas change in the form of the functions is controlled by $D/\bar{D}$ (Supplemental Figs. S.3.1 a and b[27]). Since I is un-normalized, dI/dD at $D = 0$ is the sensitivity of the signal to dose, excluding saturation effects.

B. Normalized and standardized DRCs assuming $I_T \propto D_T$

I_∞ and $\bar{D}$ may vary between samples as a function of trapping and recombination probability and changes in these with repeated measurement of a single sample. In equal-predose dose-normalized multiple aliquot measurements (Aitken,[3] p. 128), multiple activation predose measurements,[23] or the single aliquot regenerative (SAR) protocol,[24] I is divided by the response (I_T) to a fixed normalization- or "test-" dose (D_T), delivered after measurement of I, to produce a normalized signal I_N (3). If I_T accurately monitors sensitivity with respect to I, then in the idealized case of an infinitely small test-dose and $I_{T0} = 0$ (4)

$$I_N = \frac{I}{I_T}, \tag{3}$$

$$\frac{I_T}{D_T} \equiv \frac{dI}{dD}(D = 0). \tag{4}$$

For dose-normalized measurements, an approximation might still be based on the OTOR model applied separately to I and I_T, possibly with different initial filling conditions of trap and center and/or different available concentrations. However, the purpose of measuring I_N usually includes monitoring of changes in recombination probability, which are more conveniently explained by changes in the relative concentrations of holes in at least two types of recombination center, including by transfer from one to another between measurement cycles.[25] I_N may be "standardized"[8] by multiplying it by the test-dose: $I_S = D_T I_N$. Since I and I_T have units of photon counts (cts) and D_T has units of dose (Gy), I_N is dimensionless and I_S has units of dose (Gy). Making the approximation of a small but non-zero test-dose, it is evident from (2) and (4) that

$$\frac{I_T}{D_T} \approx \frac{dI}{dD}(D = 0) = \frac{I_\infty}{\bar{D}}, \tag{5}$$

$$\frac{dI_S}{dD} = \frac{dI}{dD}\frac{I_T}{D_T} = \frac{I_\infty}{\bar{D}}\frac{I_T}{D_T}e^{-D/\bar{D}} \approx e^{-D/\bar{D}}, \tag{6}$$

$$\int \frac{dI_S}{dD}.dD = I_S \approx \bar{D}(1 - e^{-D/\bar{D}}). \tag{7}$$

Thus, for the approximation of a small but finite test-dose and $I_{T0} = 0$, the gradient of the standardized DRC at $D = 0$ must approximate 1 (cf. Roberts and Duller[8]). Also, since in (1) for $D \to \infty$, $I \to I_\infty$, then in (7) $I_{\infty S} \approx \bar{D}$ (Supplemental Fig. S.3.1c, $\bar{D} = 50, 500, 5000$; S.3.1c $D_T = 0.1, 1$[27]).

C. Standardized DRCs for any fixed test response

If the approximation of a small test-dose is relinquished, the standardized signal is a function of the DRCs of both the "signal" (I) in response to the "dose" (D) and the "test-signal" (I_T) in response to the "test-dose" (D_T).[9,38] In this case, the models that may be considered for the system are the same as in Section III B, the only difference being that single saturating exponential dose responses are considered for both I and I_T (8). When D_T and I_T are constant and $I_0 = I_{T0} = 0$, (8) takes the form of a single saturating exponential as a function of D (9). At $D = 0$, $\partial I_S/\partial D = I_{\infty S}/\bar{D}$. $I_{\infty S}$ (10) is a function of D_T (constant for a given dataset), but $\bar{D}$ is not, so $I_{\infty S}$ is no longer constrained to approximately equal $\bar{D}$, and the gradient of the standardized DRC at $D = 0$ is no longer constrained to approximate unity. This is illustrated for $\bar{D} = 0.05$ and 0.5 in Supplemental Figure S3.1c[27] and for $D_T = 100$ and 1000 in Supplemental Fig. S3.2d [27]

$$I_S = D_T I/I_T = f(D, D_T) = D_T \frac{I_0 + I_\infty(1 - e^{-D/\bar{D}})}{I_{T0} + I_{T\infty}(1 - e^{-D_T/\bar{D}_T})}, \tag{8}$$

$$I_S = I_{\infty S}(1 - e^{-D/\bar{D}}), \tag{9}$$

$$I_{\infty S} = D_T \frac{I_\infty}{I_{T\infty}}\frac{1}{(1 - e^{-D_T/\bar{D}_T})}. \tag{10}$$

If I and I_T in (8) may be assumed to relate to the same DRC, then the meaning of the assumption that "I_T accurately monitors sensitivity with respect to I" (Sec. II B) in this context is clarified, i.e., $I_\infty = I_{T\infty}$ and $\bar{D} = \bar{D}_T$, and (5) is verified for small test-doses. When (10) is applied to experimental results from Burbidge *et al.*[9,39] a linear regression applied to calculated values of $\partial I_S/\partial D$ at $D = 0$, for D_T between 1 and 7 Gy, gives $y = 0.014\,x + 0.999$ which is within errors of experimental values. However, for small test-doses, the exponential of $-D_T/\bar{D}_T$ in (10) approximates $(1 - D_T/\bar{D}_T)$, and $\partial I_{\infty S}/\partial D_T$ approaches $\frac{1}{2}\,I_\infty/I_{T\infty}$, and for large test-doses the exponential of $-D_T/\bar{D}_T$ approximates zero, so $\partial I_{\infty S}/\partial D_T$ approaches $I_\infty/I_{T\infty}$ and[27]

$$\frac{D_T}{\bar{D}_T} \to 0, \quad I_{\infty S} \to \left(\bar{D}_T + \frac{D_T}{2}\right)\frac{I_\infty}{I_{T\infty}},$$

$$\frac{D_T}{\bar{D}_T} \to \infty, \quad I_{\infty S} \to D_T\frac{I_\infty}{I_{T\infty}}.$$

For a fixed normalization or test-dose (D_T) and fixed signal response (I_T) per unit test-dose (D_T) (Secs. II B and II C), any model of the system which produces a saturating exponential response is adequate, though it has been found useful to reproduce alterations in recombination probability between I and I_T. Chen et al.[40] have considered non-dose dependent changes in recombination probability by assuming that I_T followed the same DRC as I (Sec. II C) and multiplying I_T by a constant k. Changes in trapping probability were inferred to be minor, and deviations from saturating exponential dose response were accounted for by summing two signal components allocated different saturation rates.

D. DRCs for which I_T is affected by changes in signal and/or dose saturation capacity

In reality, changes in recombination probability occur between and during the measurements I and I_T, and changes in trapping probability occur between and during the irradiations D and D_T (I). This can be represented by competition for electrons in a system of two trap types and two recombination center types (2T2R model[21]), one trap type represents the source of the signal of interest, while the other represents whichever other types are present ($x = 1$ and $x = 2$ (Supplemental Sec. S1[27])), and one type of recombination center represents that which emits the measured signal (radiative), while the other represents types that do not emit or are not detected.

For negligible retrapping, the probability of electron capture by radiative recombination centers (Pr_r, Supplemental Sec. S1[27]) during measurement is the product of hole concentration (m_2) and transition coefficient for capture by the radiative center types (Am_2), divided by the sum of this for radiative and non-radiative types, all multiplied by the concentration of free electrons in the conduction band (n_c)

$$Pr_r = n_c m_2 Am_2 / (m_1 Am_1 + m_2 Am_2). \qquad (11)$$

Pr_r (11) during measurement of I (Pr_{rI}) is a function of dose (D). Pr_{rIT} is primarily a function of test or normalization dose (D_T), but for this reason, D_T is maintained constant during the experimental generation of a DRC. However, in addition to free holes produced by the test irradiation (n_v, Supplemental Sec. S1[27]) and their transfer coefficient (A_{hx}), hole concentrations at a given recombination center type (m_x) are also the function of the available concentrations of hole trapping centers prior to irradiation with the test dose (M_x, m_{x0})

$$m_x(D) = \int \{Ah_x n_v(M_x - m_x) - Am_x m_x n_c\}. dD. \qquad (12)$$

For a given value of D_T, m (12) may be different to that for the same value during the previous irradiation D, and hence Pr_{rIT} and $I_{T\infty}$ (the saturation level or "capacity" of the rate of radiative recombination) may differ from Pr_{rI} and I_∞. Initial conditions for the test irradiation are the final condition of the system following irradiation with the dose, D, and measurement, I.

In the same system, electron capture probability by traps that will contribute signal (Pt_r, Supplemental Sec. S1[27]) is

the product of the unfilled electron trap concentration ($N_1 - n_1$) and transition coefficient for electron capture (An_1) during irradiation, divided by the sum of this for all types of trap and recombination center (13)

$$Pt_r = \left\{ \frac{(N_1 - n_1)An_1}{(N_1 - n_1)An_1 + (N_2 - n_2)An_2 + m_1 Am_1 + m_2 Am_2} \right\}$$
$$= e^{-D/\bar{D}}. \qquad (13)$$

This is the proportion of traps that will produce signal which remain to be filled ($e^{-D/\bar{D}}$ in (1)). Where subject to alterations in initial conditions (N, M, n_0, m_0) between the irradiations D and D_T, then Pt_r, and hence saturation level or "capacity" for trapping is altered. Let

$$k_S = Pr_{rI_T}/Pr_{rI}, \qquad (14)$$

$$l_S = D_T ln(Pt_{rD})/Dln(Pt_{rD_T}). \qquad (15)$$

Pr_{rIT}/Pr_{rI} (14) and $D_T ln(Pt_{rDT})/Dln(Pt_{rD})$ (15) are simply related to their first order derivatives with respect to dose ($D_T = $ const) by the quotient rule (Supplemental Sec. S4.1.1[27]). For $D \to \infty$ and $D \to 0$, let

$$k_{S\infty} = \text{const.} = \frac{Pr_{rI_T}(\infty)}{Pr_{rI}(\infty)}, \qquad (16)$$

$$\bar{D}_{k_S} = \text{const.} = 1 / \left\{ \frac{1}{Pr_{rI_T}(0)} \frac{dPr_{rI_T}(0)}{dD} - \frac{1}{Pr_{rI}} \frac{dPr_{rI}(0)}{dD} \right\}. \qquad (17)$$

To satisfy conditions at both dose limits ((16) and (17)), while assuming also that any dose dependent change in k_S occurs relative to a non- or pre-dose dependent baseline level, then

$$k_S(D) - k_{S0} = k_{S\infty} - \bar{D}_{kS} \frac{dk_S}{dD}.$$

A function that satisfies this equation and the boundary conditions is (18), which describes capacitive change in radiative recombination probability. As for k_S ((16) and (17), Supplemental Sec. S4.1.2[27]), a solution to $ls(D) - l_{S0} = l_{S\infty} - \bar{D}_{lS} \, dl_S/dD$ is described by (19)

$$k_S(D) = k_{S0} + k_{S\infty}(1 - e^{-D/\bar{D}_{k_S}}), \qquad (18)$$

$$l_S(D) = l_{S0} + l_{S\infty}(1 - e^{-D/\bar{D}_{l_S}}). \qquad (19)$$

The present study considers capacitive dose dependent changes in signal level at saturation, I_∞ vs. $I_{T\infty}$, and in the average dose of signal saturation, $\bar{D}$ vs. $\bar{D}_T$

$$I_{T\infty} = k_S I_\infty,$$
$$\bar{D}_T = l_S \bar{D}, \qquad (20)$$
$$I_T = I_{T0} + k_S I_\infty(1 - e^{-D_T/l_S \bar{D}}).$$

$I_{T\infty}$ and $\bar{D}_T$ are now dose dependent variables (20), so the standardized DRC (8) no longer takes the form of a single saturating exponential. Substituting (18)–(20) into (8)

$$I_{S(kl)} = D_T \frac{\{I_0 + I_\infty(1 - e^{-D/\bar{D}})\}}{I_{T0} + I_\infty\{k_{S0} + k_{S\infty}(1 - e^{-D/\bar{D}_{k_S}})\}\left(1 - e^{-D_T/\bar{D}\{l_{S0}+l_{S\infty}(1-e^{-D/\bar{D}_{l_S}})\}}\right)}, \tag{21}$$

$$\frac{\partial_{I_{S(kl)}}}{\partial_D} = \frac{D_T}{I_T\bar{D}}e^{-D/\bar{D}} - I_S\frac{D_T I_\infty}{I_T}\left\{\frac{k_{S\infty}}{\bar{D}_{k_S}}(1 - e^{-D_T/l_S\bar{D}})e^{-D/\bar{D}_k} - \frac{k_S}{l_S{}^2}\frac{l_{S\infty}}{\bar{D}_{l_S}}\frac{D_T}{\bar{D}}e^{-D_T/l_S\bar{D}}e^{-D/\bar{D}_{l_S}}\right\}. \tag{22}$$

For illustrative purposes, $(k_{S0} - k_{S\infty})/k_{S0}$ and $(l_{S0} - l_{S\infty})/l_{S0}$ were chosen to be -0.01 (Figs. 1(a) and 1(c)) and 100 (Figs. 1(b) and 1(d)). The effect of changes in recombination probability between the beginnings of the measurements I and I_T, and changes in trapping probability between the beginnings of the irradiations D and D_T, is to transfer the DRC from one saturating exponential trajectory to another. Since I_T was measured subsequent to I, the transfer is worked on I_S through change in I_T as a function of D (Fig. 1 insets). Any increase or decrease of k_S, between $D = 0$ and $D = \infty$, produces similar changes in I_T and hence the inverse effect on I_S. l_S scales the denominator of a negative exponent in a saturating exponential term (21), so the effect of increasing l_S is greater than that of decreasing it. Six generalized forms of DRC (0/ to 5/) are summarized in Table I, along with the

main parameter constraints in (21) that control their appearance.

E. Changes in signal and/or dose saturation capacity in non-normalized DRCs

If the test-dose in (21) were before the dose, then k and l apply to I and not to I_T. If the test-irradiation and measurement were removed, then change in recombination or trapping probability would apply to I, relative to unity, and so manifest in the un-normalized dose response

$$I = I_0 + kI_\infty(1 - e^{-D/l\bar{D}}). \tag{23}$$

Unlike k_S and l_S in (21), in (23), k and l (Supplemental Sec. S4.2[27]) are orthogonal: k only affects I_∞ and l only affects $\bar{D}$. This indicates a basic difference between dose-normalized and un-normalized DRCs. With (23), it is possible to produce all the forms (0/ to /5) in Table I, but $k \neq 0$ is now required to produce any DRC where $I(D \to \infty) \neq I_\infty$, and $k_\infty < 0$ is required to obtain non-monotonic DRCs. Since they are applied directly to I and not via I_T, in (23), the roles of k and l are reversed with respect to (21): k now produces the forms in Figs. 1(c) and 1(d), and l produces the forms in Figs. 1(a) and 1(b) (when $k_\infty < 0$).

III. EXAMPLES OF APPLICATION TO SIMULATED AND EXPERIMENTAL RESULTS

A. Two trap two recombination center model

Lawless et al.[21] obtained curves similar to Fig. 1(b)— $\bar{D}_k$ (21) = 5000 and Fig. 1(c)—$\bar{D}_l$ (21) = 5000, using a one trap two recombination center (1T2R) model and a two trap two recombination center (2T2R) model, for non-normalized DRCs in cases dominated by competition during excitation (called irradiation in the present study) and measurement. In the present study, a 2T2R model was implemented in Wolfram Mathematica 10.0, based on Pagonis et al.[19] with baseline parameter values rounded from Lawless et al.[21] (Table II; Ref. 27). Measurement of maximum TSL was retained, since it behaves similarly to integral OSL[6] and present interest is in generalized behavior. The electron traps N_1 were measured by TSL from radiative hole traps M_2. Initial trapped charge populations were set to zero (cf. Chen et al.[20]). Under these conditions, competition for trapping of electrons in N_1 during irradiation is dominated by the recombination centers m_1 and m_2, so retrapping probability is low and TSL kinetics approximate first order (cf. Pagonis et al.[5]), while the total capacity for electron trapping or recombination is dominated by N_1 and M_1. Since $An_1 = Am_1$ and
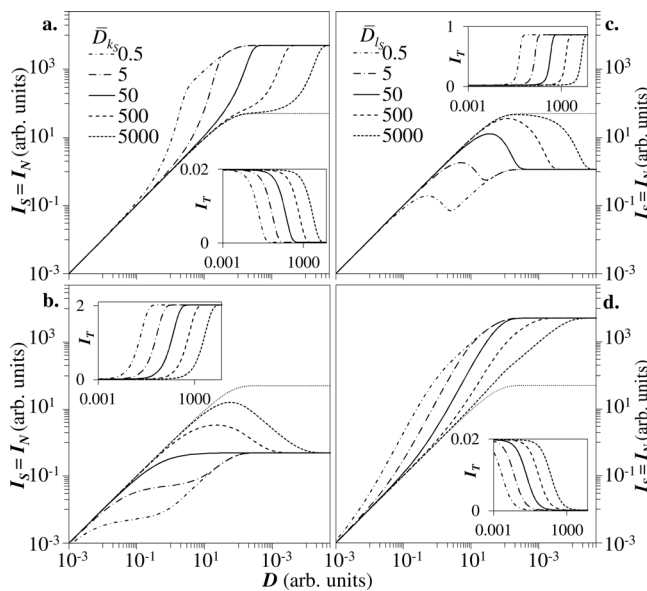

FIG. 1. Variation in the form of $I_S(D)$ (21) with $\bar{D}_{kS}$ ($l_{S\infty}$ set to 0) for (a) $k_{S\infty} = -0.99$ and (b) $k_{S\infty} = 101$ and with $\bar{D}_{lS}$ ($k_{S\infty}$ set to 0) for (c) $l_{S\infty} = -0.99$ and (d) $l_{S\infty} = 101$. The plots show how the form of (21) changes for different rates and magnitudes of dose (D) dependent change in (a) and (b) relative signal saturation capacity between the measurement of dose response $I(D)$ and the measurement of the response to the normalization or test-dose (D_T), I_T, and in (c) and (d) relative dose saturation capacity between the start of irradiation with the dose, D, and the start of irradiation with the normalization or test-dose, D_T. This is achieved by varying $\bar{D}_{kS}$ or $\bar{D}_{lS}$ from 0.5 to 5000, relative to a $\bar{D}$ value of 50, for the different values of $k_{S\infty}$ or $l_{S\infty}$. In all cases, $\bar{D}$, $\bar{D}_T = 50$; I_∞, k_{S0}, l_{S0}, $D_T = 1$; I_0, I_{T0}, = 0. Since $D_T = 1$, $I_S = I_N$. The dotted line indicates the DRC for $k_{S\infty} = 0$ ((a) and (b)) or $l_{S\infty} = 0$ ((c) and (d)), i.e., no change in relative signal and dose saturation capacity. Inset is the dose dependence of change, relative to I, in a subsequently measured normalization or test-dose response, I_T, which produces the dose dependent change in the DRCs. Calculated examples are presented in arbitrary units, but D and so I_S may be considered to be in Gy.

TABLE I. Summary of the different forms of the standardized DRC observed in curves calculated based on (21) and (23), illustrated in the listed figures and tables (and see Sec. II D).

Form of DRC	Conditions I_S, Eq. (21)	I, Eq. (23)	Examples
0/ Saturating exponential increase to saturation	$k_{S\infty} = l_{S\infty} = 0$[a]	$k_\infty = l_\infty = 0$	Fig. 1(b), $\bar{D}_{kS} = 50$; Fig. 2/Table II (a-iv); Fig. 3/Table III (b-i) and (b-ii).
1/ Superlinearity followed by "two phase saturation"	$k_{S\infty} < 0, \bar{D}_{kS} < \bar{D}; l_{S\infty} > 0$	$k_\infty > 0, l_\infty < 0, \bar{D}_k < \bar{D}$	Fig. 1(a), $\bar{D}_{kS} = 0.5$ and 5; Fig. 1(d); Fig. 3/Table III (b–iii).
2/ Sublinearity followed by "accelerated saturation"	$k_{S\infty} < 0, \bar{D}_{kS} > \bar{D}$	$k_\infty > 0, l_\infty > 0, \bar{D}_k < \bar{D}$	Fig. 1(a), $\bar{D}_{kS} = 500$ and 5000.
3/ Early onset sublinearity followed by "subdued saturation"	$k_{S\infty} > 0, \bar{D}_{kS} < \bar{D}; l_{S\infty} < 0, \bar{D}_{lS} < \bar{D}$	$k_\infty < 0, l_\infty > 0, \bar{D}_k < \bar{D} < \bar{D}_l$	Fig. 1(b), $\bar{D}_{kS} = 0.5$ and 5; Figs. 2/Table II (a-i)–(a-iii).
4/ Peak followed by "negative saturation"	$k_{S\infty} > 0, \bar{D}_{kS} > \bar{D}; l_{S\infty} < 0, \bar{D}_{lS} \geq \bar{D}$	$k_\infty < 0, l_\infty < 0, \bar{D}_k \geq \bar{D}_l > \bar{D}; k_\infty \leq l_\infty \ll 0 \ll I_\infty, \bar{D}_k < \bar{D}_l \ll \bar{D}$	Fig. 1(b), $\bar{D}_{kS} = 500$ and 5000; Fig. 1(c), $\bar{D}_{lS} = 50, 500$ and 5000; Fig. 2/Table II (a-v), (a-vi), (b-iv)−(b-vi); Fig. 3/TABLE III (a-ii).
5/ Peak and trough followed by sublinear increase to saturation	$l_{S\infty} \ll 0, \bar{D}_{lS} < \bar{D}$	$k_\infty \leq l_\infty \ll 0 \ll I_\infty, \bar{D}_l \leq \bar{D}_k \ll \bar{D}$	Fig. 1(c), $\bar{D}_{lS} = 0.5$ and 5; Fig. 2/Table II (b-i)–(b-iii); Fig. 3/Table III (a-iii).

[a]$l_{S\infty} = 0$ or $\bar{D}_{lS} \to \infty$ and $k_{S\infty} = e^{-1} - 1$, $\bar{D}_{kS} = \bar{D}/ - ln[(\grave{I}_\infty e^{-1} - (1 + \grave{I}_\infty - I_\infty) e^{-I\infty/\grave{I}\infty})/(I_\infty - \grave{I}_\infty + e^{-1})]$, where $\grave{I}_\infty$ is the apparent or measured signal level at saturation.

$N_1 = M_1$, the system is at the boundary of producing a non-monotonic DRC.[21]

M_1 was multiplied by 2 to produce an excess of non-radiative hole traps and so permit the generation of non-monotonic responses.[21] To approximate the forms of DRC in Fig. 1(b) ($\bar{D}_{kS}$ (21) varied), while maintaining signal level at saturation approximately constant, An {An_1, An_2} and the reciprocal of Am {$1/Am_1$, $1/Am_2$} were multiplied by orders of 2 between −1 and 2 (Table II and Fig. 2(a)). A factor of $2^{1/2}$ negated the 2 times excess of M_1 and yielded a simple saturating exponential DRC (form 0/—Table I). Factors greater and less than $2^{1/2}$ produced forms 4/ and 3/. The peaks in form 4/ were less extended on the irradiation-time axis than those obtained on the dose axis using (21) (Fig. 1(b)), and superlinear increase was evident at low irradiation times. The forms of DRC in Fig. 1(c) ($\bar{D}_{lS}$ (21) varied) were approximated using curve v* (Table II), then multiplying N_1 and M_1 by orders of 10 between −4 and 1 (Table II and Fig. 2(b)). R was changed in parallel, to make $\bar{D}_k$ and $\bar{D}_l$ (23) approximately constant. As N_1, M_1, and R were decreased, the decline of the peak moved from the saturated region of the DRC into a region of continued increase. For the present base parameter values (Table II; Ref. 27), this pattern was specific to severe reduction of both N_1 and M_1 in parallel and not N_2. However, while variation of N_1 and M_1 approximated the effects of varying $\bar{D}_{lS}$ (21) broadening of the peak was not obtained for high concentrations, and the peak becomes a shoulder as N_1 and M_1 decrease to become similar to N_2 and M_2, then the DRC shifts.

The 2T2R data in Fig. 2(a) were approximated with (23) by assuming high I_∞, varying $\bar{D}_k$ by the same proportions as An/Am and varying l_∞ as a negative power of this ($\bar{D}_k^{-0.8}$), with $I_0 = 0$, $k_0 = l_0 = 1$, and $\bar{D}$, $\bar{D}_l$, and k_∞ approximately constant (An/Am (i)–(iv) of Table II). l_∞ was positive

TABLE II. Parameters varied in calculation of the DRCs plotted in FIG. 2, using the 2T2R model and (23). The complete base parameter set for the 2T2R model is given in Supplemental Sec. S2.[27] For (23), $I_0 = 0$ and $k_0 = l_0 = 1$ in all cases.

| 2T2R	Base	An/Am			(Fig. 2(a))					N_1 and M_1			(Fig. 2(b))		
		i	ii	iii	iv	v	vi	v*	vi*	i	ii	iii	iv	v	vi
2T2R	**Base**														
An_1	10^{-17}	0.5	0.707	1	1.41	2	4	2	4	2	2	2	2	2	2
An_2	10^{-18}	0.5	0.707	1	1.41	2	4	2	4	2	2	2	2	2	2
Am_1	10^{-17}	2	1.41	1	0.707	0.5	0.25	0.5	0.25	0.5	0.5	0.5	0.5	0.5	0.5
Am_2	10^{-16}	2	1.41	1	0.707	0.5	0.25	0.5	0.25	0.5	0.5	0.5	0.5	0.5	0.5
N_1	10^{21}	1	1	1	1	1	1	1	1	0.0001	0.001	0.01	0.1	1	10
M_1	10^{21}	2	2	2	2	2	2	2	2	0.0002	0.002	0.02	0.2	2	20
R	10^{19}	1	1	1	1	1	1	1	1	0.001	0.01	0.1	1	10	100
Eq. (23)	**Base**														
I_∞	10^{13}	392	361	382	381	380	380	3820	3 700 000	619	3660	380	382	382	382
$\bar{D}$		66	61	64	62	62	62	640	600 000	1961	825	73	64	64	64
k_∞		−0.60	−0.58	−0.61	−0.62	−0.64	−0.72	−0.96	−1.00	−0.76	−0.95	−0.96	−0.96	−0.96	−0.96
$\bar{D}_k$		6.3	13	26	51	100	200	34	11	173	4.0	3.9	3.4	3.4	3.3
l_∞		3.98	2.03	0.64	0.00	−0.64	−0.72	−0.90	−1.00	−0.78	−0.83	−0.84	−0.90	−0.90	−0.91
$\bar{D}_l$		100	100	100	100	100	100	41	12	2.1	3.9	3.9	4.1	4.1	4.0
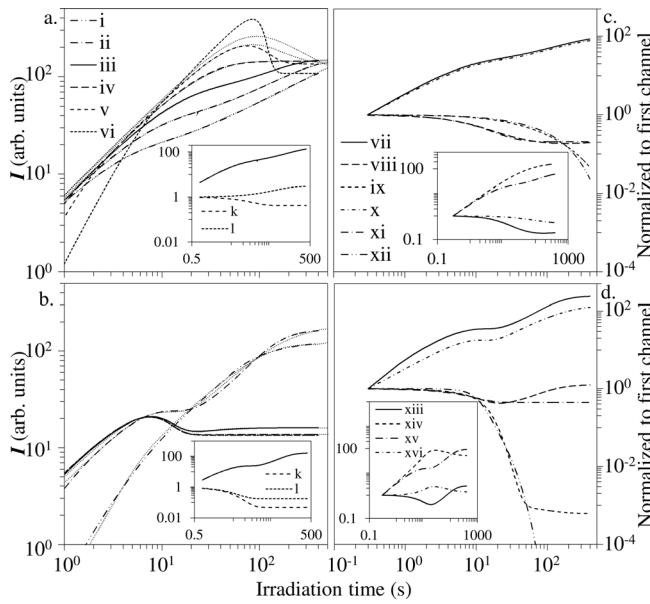
FIG. 2. *I* vs. Irradiation time (s) simulated with the 2T2R model as a function of varying (a) relative electron trapping probability associated with storage and recombination, *An/Am*, for $R = 10^{19}$ (pairs), and (b) electron trapping probability in the dominant storage and recombination centers, N_1 and M_1, for values of R between 10^{16} and 10^{21} (pairs) (i)–(vi) of Table II). Curves calculated using (23), and adjusted by minimizing Chi-squared using the Excel solver, are shown as fine dotted lines (Table II). Inset are the plots of *I*, *k*, and *l* (23), for (a-ii) and (b-ii). In (c) and (d), parameters obtained from the 2T2R model following relaxation are plotted alongside curves calculated from *I*, *k* and *l* (23) normalized to the first channel (t = 0.3 s), for the same examples (a-ii) and (b-ii), In the main plots (c) and (d) are shown curves obtained following relaxation: vii *I*(2T2R), (viii) $Am_2m_2/(Am_1m_1+Am_2m_2)$ (24), (ix) $An_1(N_1 - n_1)/(An_1(N_1 - n_1) + An_2(N_2 - n_2) + Am_1m_1+Am_2m_2)$, (25), (x) *I*(23), (xi) k^κ (24), and (xii) $\exp(-D/l^\lambda \bar{D})$ (19) and (25). In (c) $\kappa = 1.8$, $\lambda = 0.5$. In (d) $\kappa = 0.27$, $\lambda = 2.7$. Inset in (c) and (d), $Am_2m_2/n_c(Am_1m_1 + Am_2m_2 + An_1(N_1 - n_1) + An_2(N_2 - n_2))$ (26) ((xiii) and (xv)), and n_c ((xiv) and (xvi)) and are shown before ((xiii) and (xiv)) and after ((xv) and (xvi)) relaxation.

for low *An/Am*, so that $l\bar{D}$ increased as a function of dose (Fig. 2(a) inset), and the 2T2R data were closely reproduced ((i), (ii), and (iii) of Fig. 2(a)). Low dose superlinear regions needed to be described separately from the peaks using (23).

Fits to the peaks for high *An/Am* were improved by increasing the magnitudes of I_∞, $\bar{D}$, k_∞, and l_∞, and reducing both the magnitude and difference between $\bar{D}_k$ and $\bar{D}_l$ (v* and vi* of Table II). The N_1 and M_1 data in Fig. 2(b) were closely reproduced by declines in *k* and *l* at different rates, produced by gradual 10%–20% increase in $\bar{D}_k$ and l_∞ as N_1, M_1, and R were decreased (N_1 and M_1, (vi)–(ii) of Table II), then increases in the orders of magnitude of $\bar{D}$ and I_∞ ((iii)–(i)), and finally also large changes in $\bar{D}_l$ and $\bar{D}_k$ with shift of the DRC (i).

k and *l* (23) are closely related to variation in parameters calculated from the 2T2R model (Figs. 2(c) and 2(d)). *k* approximates variation with irradiation time of the relative radiative recombination probability per unit charge in the conduction band (24) (cf. Eqs. (11) and (14)), though only if the magnitude is adjusted by raising *k* by κ (Figs. 2(c) and 2(d), curves (viii) and (xi); Supplemental Sec. S4.3[27]). Similarly, *l* approximates variation of the quotient of dose (irradiation time) and the natural logarithm of the normalized relative electron capture probability in the traps that will contribute signal (25) (cf. Eqs. (13) and (15)); though only if the magnitude is adjusted by raising *l* by λ (Figs. 2(c) and 2(d), curves (ix) and (xii); Supplemental Sec. S4.3[27]). I/I_0 was well approximated by (26) when *j* was based on values obtained prior to relaxation (Figs. 2(c) and 2(d), curves (vii), (x), and (xiii); Supplemental Sec. S4.3[27]). Thus, the signal that would subsequently be obtained was well approximated by the relative electron capture probability in radiative recombination centers vs. all recombination and trapping centers, during irradiation. Then, following relaxation, $j = (24) \approx k^\kappa$, the relative recombination probability in radiative vs. all recombination centers during measurement (Figs. 2(c) and 2(d), curves (xi) and (xv))

$$k^\kappa \approx n_{c_0}Pr_{rI(D)}/n_cPr_{rI_0}, \tag{24}$$

$$l^\lambda \approx -D/\bar{D}\ln(Pt_{rD}/Pt_{r(D=0)}), \tag{25}$$

$$j = \frac{\left(Am_2m_2/\left[nc\{(N_1 - n_1)An_1 + (N_2 - n_2)An_2 + m_1Am_1 + m_2Am_2\}\right]\right)}{\left(Am_2m_2/\left[nc\{(N_1 - n_1)An_1 + (N_2 - n_2)An_2 + m_1Am_1 + m_2Am_2\}\right]\right)_{D=0}}. \tag{26}$$

Change in *An/Am* or N_1 and M_1 most strongly affects the parameters $\bar{D}_k$ and l_∞. Since the present choice of 2T2R parameter values makes electron capture by recombination centers a major competitor for electron capture in electron traps, changes in trapping probability neither simply relate to electron traps nor changes in recombination probability to recombination centers. However, it is notable that (23) requires $k_\infty < 0$ to produce non-monotonic forms, while the 2T2R model requires $M_1 > N$. In (23), this means that I_∞ must be large, but the equation cannot then also account for low dose superlinearity in 2T2R results, which were calculated assuming initial trapped charge concentrations to be zero. For fitted/forced cases with very high I_∞ values (* in

Table II), *I* and kI_∞ display a similar relationship to that illustrated in Fig. 2 of Chen *et al.*[20] with respect to signal and decline in an initially high radiative center population, i.e., these cases are dominated by the initial radiative center population m_0, and I_∞ reflects this.

B. OSL, TTOSL, and phototransferred thermoluminescence (PTTL)

Heating between OSL and TTOSL measurement is designed to thermally transfer charges into traps previously emptied by OSL (hence, TTOSL). Continued increase of TTOSL signals has been observed beyond saturation of OSL
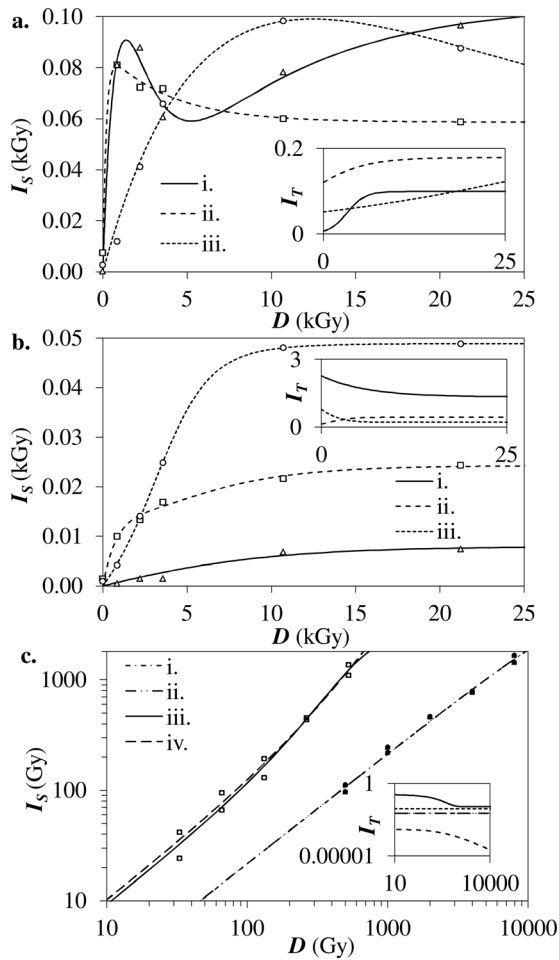
FIG. 3. Examples of experimental data for multi-kGy DRCs for quartz, selected from Burbidge *et al.*[10,33] standardized, and fitted using (21) by varying $\bar{D}$ and a limited number of other parameters (Table III). (a) OSL standardized OSL and (b) OSL standardized TTOSL, both from a TTOSL measurement sequence. (c) Beta standardized α and β OSL DRCs from milled quartz.

signals.[10,41–44] DRCs exhibiting superlinear (form 1/—Table I) and non-monotonic behavior (forms 4/ and 5/—Table I) have been reported[10] for OSL measurements made within a multiple aliquot regenerative TTOSL protocol (Fig. 3(a)). The OSL DRCs (Fig. 3(a)) can be well approximated using various combinations of free parameters in (21). The combination with the least degrees of freedom used $\bar{D}$, k_{S0}, $l_{S\infty}$, and $\bar{D}_{lS}$, i.e., non-dose dependent increase in relative signal saturation capacity and dose dependent decrease in relative dose saturation capacity (Table III—(a-i), (a-ii), (a-iii)). Although apparently simpler in form, the TTOSL DRCs from same subsamples in the same measurement sequence (Fig. 3(b)) required more specific combinations of free parameters for fitting ((21); Table III—(b–i), (b-ii), (b-iii)): a very large increase in nondose-dependent signal saturation capacity (k_{S0}) between I and I_T, and not in dose saturation capacity l_{S0}. Two of the three were also well fitted using dose dependent decreases in $l_{S\infty}$, similar to the OSL DRCs, but two required dose dependent decreases in k_S. While the TTOSL DRCs exhibit continued monotonic increases to higher doses than those of OSL, the $\bar{D}$, $\bar{D}_{kS}$, and $\bar{D}_{lS}$, values obtained from them were commonly lower.

In contrast to OSL the TTOSL signal is, by definition, produced from retrapped electrons and so a second order effect, which were explicitly excluded from the derivation of (21). Thus, in application of (21) to TTOSL data, the quantities of retrapped electrons (and holes) that will subsequently produce the (TT)OSL signal are assumed to be proportional to those trapped in the "TT traps" prior to thermal transfer. These proportions are included in k_{S0} and l_{S0}. If the retrapped proportions vary with dose, then second order effects on k_S and l_S may render (18) and (19) inadequate for description of the observed variations, and hence the DRC. The experimental datasets in Fig. 3 are sparse, but they do indicate that the principal difference between the OSL and TTOSL response to dose is best described as difference and change in signal (k_S), not dose (l_S) at saturation. Since the principal effect of OSL measurement is to remove electrons from optically sensitive trapping centers, the effect on any subsequent (TT)OSL measurement may be viewed as a change in recombination probability resulting from a difference in the filling of traps, instead of recombination centers. These results indicate similar $\bar{D}$ to that of the main OSL signal and so support the interpretation that any differences in trapping probability during irradiation for the two signals are small,

TABLE III. Parameter values used in (21), to calculate the curves plotted in Fig. 3.

Fig. 3	Dose response characteristic									
	a-i	a-ii	a-iii	b-i	b-ii	b-iii	c-i	c-ii	c-iii	c-iv
Type	β normalized β, OSL in TTOSL sequence			β normalized β, TTOSL			β normalized α or β, OSL			
f	(k_{S0}, l_S)	(k_{S0}, l_S)	(k_{S0}, l_S)	(k_S)	(k_{S0}, l_S)	(k_S, l_S)	$(\alpha\, k_{S0})$	$(\alpha\, l_{S0})$	$(\beta\, k_S)$	$(\beta\, l_S)$
D_T	0.01	0.01	0.01	0.01	0.01	0.01	66	66	66	66
$I_0 = I_{T0}$	0	0	0	0	0	0	0	0	0	0
I_∞	1	1	1	1	1	1	1	1	1	1
$\bar{D}$	8.4	0.2	8.4	5.4	4.4	2.8	34 383	34 392	422	95 333
k_{S0}	5.2	2.4	41	1172	60	60	4.63	1	1.2	1
$k_{S\infty}$	0	0	0	−487	0	−55	0	0	−1	0
$\bar{D}_{kS}$	1	1	1	6.0	1.0	1.5	1	1	220	1
l_{S0}	1	1	1	1	1.1	0.28	1	0.22	1	1
$l_{S\infty}$	−0.94	−0.34	−0.84	0	−0.75	−0.19	0	0	0	8768
$\bar{D}_{lS}$	1.2	3.8	21	1	1.4	2.1	1	1	1	3.5×10^6

compared with the effect of removal of much trapped charge by OSL measurement prior to TTOSL measurement.[44] TTOSL appears similar to SAR OSL measurements on quartz using preheats of sufficiently high temperature to erode the OSL signal for I (but not I_T): where no superlinear changes are considered, only signal level varies and the average dose of saturation is unaffected. Recombination during OSL measurement and the "TTheat" (prior to TTOSL) use up a proportion of trapped holes, particularly the centers with the largest electron capture cross-sections, while the "TTheat" transfers a fraction of the remainder into radiative centers. This is expected to be more significant for the larger doses used by Burbidge *et al.*[10] than was observed by Stokes[45] and is considered the source of the observed superlinear effects and hence apparent (monotonic) signal increases to higher doses than OSL.

PTTL is another type of signal derived from re-trapped charge.[2,46] PTTL in quartz has been related to charge transfer *via* the conduction band between apparently similar dominant traps and centers as TSL, OSL, and so TTOSL.[47,48] PTTL from the "110 °C" TSL trap could be measured at a similar temperature to OSL during the "TTheat" in a TTOSL protocol and also be normalized to an OSL test response. In this case, PTTL and TTOSL DRCs should be similar, since transfer processes involving large amounts of charge are shared. Differences would obtain from $\bar{D}$ of the OSL vs. TT "storage" traps (small for the present samples), and retrapping probability for TSL vs. the product of TT and OSL (i.e., differences in k_{S0}). However, any thermal activation during the "TTheat" could also be reduced in a PTTL-only protocol.

C. Alpha efficiency and superlinearity

The OSL and TSL signal response of quartz to α radiation is commonly found to be matched by a β dose ca. 0.01 times the α dose, when the β response is linear ("α efficiency" and k_{eff};[49] i.e., for $D \approx 0$, see Sec. II C). This difference relates principally to saturation of trapped charge proximal to tracks produced by high LET particles, and so to differences in trapping probability.[15,18] Experimental results are affected by supralinearity of the β response.[15,50,51] The α response of quartz is considered to exhibit only saturation (i.e., sublinearity) and at higher doses than β.[3] Burbidge *et al.*[33] observed α efficiencies of 0.1 (high dose) to 0.3 (low dose) for milled quartz, by interpolating β-dose normalized α and β DRCs (Fig. 3(c)). These high values were ascribed to high defect concentrations produced by milling. However, no attempt was made to evaluate supralinearity.

The multi-kGy α DRC in Figs. 3(c-i) and 3(c-ii)[33] only exhibits saturation: fits using (21) only require freedom in $\bar{D}$ and a multiplier (l_{S0} or k_{S0}) to evaluate the α efficiency relative to the β normalization dose, $l_{S0} = 1/k_{S0} = 0.22$ (Table III—(c–i) and (c-ii)). Use of l_{S0} is more logical to describe the relative trapping probability of α dose response and β test dose response, but the α DRC is sufficiently simple that it can be described by either. The β DRC exhibits superlinearity in the range producing OSL signals similar to the α DRC (Figs. 3(c-iii) and 3(c-iv)). Again, the form is relatively simple and can be described by varying $\bar{D}$ and the parameters of

k_S or l_S, but the values obtained using l appear extreme: use of k_S is more logical to describe relative recombination probability, and change in this, between the β dose response and the β test dose response. An α efficiency of 0.22 was obtained by fitting only the α DRC relative to a single β test dose value, effectively by signal matching. However, the ratio $\bar{D}_\beta / \bar{D}_\alpha$ (Table III, $\bar{D}$ (c-iii)/(c-i) or (c-ii)) gives the relative trapping probability for the α and superlinearity-corrected-β DRCs: this is 0.01.

IV. CONCLUSIONS

The present study elaborates an approach to describing luminescence DRCs, which, using only the consequences of basic physical models for signal production, can help to indicate what type mechanism is involved in producing a particular form of DRC. A simple combination of dose dependent saturating exponential functions was able to reproduce most observed features of luminescence DRCs quantitatively, as well as to describe the effects of radiations of different qualities on the dosemeter. Analytical functions describing capacitive change in recombination and trapping probability, which transfer the DRC from one saturating exponential trajectory to another, were related directly to parameters obtained from numerical simulation. Signal was sourced from a single trap and produced all forms of supralinearity, including non-monotonic DRCs. Although sums of signal components representing contributions from different electron trapping states may be present, this assumption is not necessary to explain the forms of currently observed DRCs. While this work has focused on radiation dosimetry using luminescence measurements, the approach is expected to be relevant to other dosimetric systems with first order kinetics, following exponential trajectories.

[1]C. I. Burbidge, Spectrosc. Lett. **45**, 118–126 (2012).
[2]S. W. S. McKeever, *Thermoluminescence of Solids* (Cambridge University Press, 1985).
[3]M. J. Aitken, *Thermoluminescence Dating* (Academic Press, London, 1985).
[4]R. Chen and S. G. E. Bowman, Eur. PACT J. **2**, 216–235 (1978).
[5]V. Pagonis, R. Chen, and J. L. Lawless, J. Lumin. **132**, 1446–1455 (2012).
[6]R. Chen and P. L. Leung, J. Appl. Phys. **89**, 259 (2001).
[7]R. Grün, Radiat. Meas. **26**, 297–302 (1996).
[8]H. M. Roberts and G. A. T. Duller, Radiat. Meas. **38**, 241–252 (2004).
[9]C. I. Burbidge, G. A. T. Duller, and H. M. Roberts, Radiat. Meas. **41**, 278–288 (2006).
[10]C. I. Burbidge, S. I. Cabo Verde, A. C. Fernandes, M. I. Prudêncio, M. L. Botelho, M. I. Dias, and G. O Cardoso, Radiat. Meas. **46**, 860–865 (2011).
[11]G. W. Berger, Ancient TL **8**, 23–25 (1990).
[12]V. Mejdahl, Nucl. Tracks Radiat. Meas. **10**, 605–608 (1985).
[13]E. J. Rhodes, C. B. Ramsey, Z. Outram, C. Batt, L. Willis, S. Dockrill, and J. Bond, Quat. Sci. Rev. **22**, 1231–1244 (2003).
[14]R. Chen and S. W. S. McKeever, Radiat. Meas. **23**, 667–673 (1994).
[15]G. O. Sawakuchi, E. G. Yukihara, S. W. S. McKeever, E. R. Benton, R. Gaza, Y. Uchihori, N. Yasuda, and H. Kitamura, J. Appl. Phys. **104**, 124903 (2008).

[16]E. F. Mische and S. W. S. McKeever, Radiat. Prot. Dosim. **29**, 159–175 (1989).

[17]C. Charitidis, G. Kitis, C. Furetta, and S. Charalambous, Nucl. Instrum. Methods Phys. Res., Sect. B **168**, 404–410 (2000).

[18]Y. S. Horowitz, O. Avila, and M. Rodriguez–Villafuerte, Nucl. Instrum. Methods Phys. Res., Sect. B **184**, 85–112 (2001).

[19]V. Pagonis, G. Kitis, and C. Furetta, *Numerical and Practical Exercises in Thermoluminescence* (Springer, 2006).

[20]R. Chen, V. Pagonis, and J. L. Lawless, J. Appl. Phys. **99**, 033511 (2006).

[21]J. L. Lawless, R. Chen, D. Lo, and V. Pagonis, J. Phys. C: Condens. Matter **17**, 737–753 (2005).

[22]A. G. Wintle, Radiat. Meas. **27**, 769 (1997).

[23]R. Chen, Counc. Eur. PACT J. **3**, 325–335 (1979).

[24]A. S. Murray and A. G. Wintle, Radiat. Meas. **32**, 57–73 (2000).

[25]J. Zimmerman, J. Phys. C: Solid State Phys. **4**, 3265–3276 (1971).

[26]A. K. Singhvi, S. C. Stokes, N. Chauhan, Y. C. Nagar, and M. K. Jaiswal, Geochronometria **38**, 231–241 (2011).

[27]See supplementary material at http://dx.doi.org/10.1063/1.4927214 for a glossary of notation used through the manuscript, a list of the Mathematica program file used in calculations for the 2T2R model, two figures, and supplementary derivations.

[28]D. K. Koul, G. Adamiec, and M. P. Chougaonkar, J. Phys. D: Appl. Phys. **42**, 115110 (2009).

[29]M. Martini, A. Paleari, G. Spinolo, and A. Vedda, Phys. Rev. B **52**, 138–142 (1995).

[30]N. Itoh, D. Stoneham, and A. M. Stoneham, J. Appl. Phys. **92**, 5036–5044 (2002).

[31]M. Martini and A. Galli, Phys. Status Solidi B **4**, 1000 (2007).

[32]R. B. Galloway and H. J. Napier, Ancient TL **12**, 43–49 (1994).

[33]C. I. Burbidge, M. I. Dias, M. I. Prudêncio, L. Rebêlo, G. O, Cardoso, and P. Brito, Radiat. Meas. **44**, 494–500 (2009).

[34]M. Jain and C. Ankjærgaard, Radiat. Meas. **46**, 292–309 (2011).

[35]J. Garcia–Guinea, V. Correcher, A. Delgado, and L. Sanchez-Muñoz, Radiat. Meas. **37**, 473–477 (2003).

[36]M. S. Akeslrod, V. S. Kortov, and E. A. Gorelova, Radiat. Prot. Dosim. **47**, 159–164 (1993).

[37]A. Khawam and D. R. Flanagan, Phys. Chem. B **110**, 17315–17328 (2006).

[38]Z. Shen and B. Mauz, Radiat. Meas. **46**, 649–654 (2011).

[39]C. I. Burbidge, Ph.D. thesis, Aberystwyth University, 2003.

[40]G. Chen, A. Murray, and S.-H. Li, Radiat. Meas. **33**, 59–63 (2001).

[41]B. Li and S.-H. Li, J. Phys. D: Appl. Phys. **39**, 2941–2949 (2006).

[42]V. Pagonis, R. Chen, and A. G. Wintle, J. Phys. D: Appl. Phys. **40**, 998–1006 (2007).

[43]G. Adamiec, R. M. Bailey, X. L. Wang, and A. G. Wintle, J. Phys. D: Appl. Phys. **41**, 135503 (2008).

[44]Z. X. Shen, B. Mauz, and A. Lang, J. Phys. D: Appl. Phys. **44**, 295405 (2011).

[45]S. Stokes, Radiat. Meas. **23**, 601–605 (1994).

[46]M. Moscovitch, AIP Conf. Proc. **1345**, 323 (2011).

[47]A. G. Wintle and A. S. Murray, Radiat. Meas. **27**, 611–624 (1997).

[48]M. Martini, M. Fasoli, and A. Galli, Radiat. Meas. **44**, 458–461 (2009).

[49]D. W. Zimmerman, Radiat. Eff. **14**, 81–92 (1972).

[50]M. J. Aitken, Ancient TL **3**, 22–25 (1985).

[51]B. Mauz, S. Packman, and A. Lang, Ancient TL **24**, 47–52 (2006).